Greek Letters

α = relative permeability
θ = dialysis coefficient defined in Eq. 9
ρ = defined in Eq. 40
σ = defined in Eq. 41

Subscripts

A = more permeable solute
B = less permeable solute
I = region in a dialyzer
II = region in a dialyzer
b = bottom
d = overhead

Abbreviations

CDP = concentrator-dialyzer pair (Figure 6)
DSA = dialysis selectivity amplifier (Figure 9)

LITERATURE CITED

Babb, A. L., C. J. Maurer, D. L. Fry, P. R. Popovich, and R. E. McGee, "The determination of membrane permeabilities and solute diffusivities to hemodialysis," *Chem. Eng. Prog. Symp. Ser.*, **64**(84), 59 (1968).

Breslau, B. R., E. A. Agranat, A. J. Testa, S. Messinger, and R. A. Gross, "Hollow fiber ultrafiltration," *Chem. Eng. Prog.*, **71**, 74 (1975).

Clusius, K. and G. Z. Dickel, "Separation tube: Z new method of gas and isotope separation by thermal diffusion," *Z. Physik. Chem.*, **44**, 397 (1939).

Colton, C. K., A. Smith, E. W. Merrill, and P. C. Farrell, "Permeability studies with cellulosic membranes," *J. Biomed. Mater. Res.*, **5**, 459 (1971).

Fenske, M. R., "Composition of straight-run Pennsylvania gasoline," *Ind. Eng. Chem.*, **24**, 482 (1932).

Hertz, G. L., "A new method for the separation of gas mixtures by diffusion," *Physik. Z.*, **23**, 433 (1922).

Kedem, O. and A. Katchalsky, "Thermodynamic analysis of the permeability of biological membranes to nonelectrolytes," *Biochim. Biophys. Acta.*, **27**, 229 (1958).

Kimura, S., S. Sourirajan, and H. Ohya, "Stagewise reverse osmosis design," *I&EC Proc. Des. Dev.*, **8**, 79 (1969).

Kirjassof, D., S. Pinto, and C. Hoffman, "Ultrafiltration of Latex solutions," *Chem. Eng. Prog.*, 58 (Feb., 1980).

Klein, E., E. F. Holland, A. Lebouf, A. Donnaud, and J. K. Smith, "Transport and mechanical properties of hemodialysis hollow fibers," *J. Memb. Sci.*, **1**, 371 (1976).

Klinkowski, P. R., "Ultrafiltration: An emerging unit operation," *Chem. Eng.*, 165 (May 8, 1978).

Maier, C. G., "Separation of gases by diffusion," *J. Chem. Phys.*, **7**, 854 (1939).

Mahon, H. I. and B. J. Lipps, "Hollow fiber membranes," "Encyclopedia of polymer science and technology," **5**, 258, Wiley, New York (1971).

Michaels, A. S., "Analysis of membrane transport devices," *Trans. Amer. Soc. Art. Int. Organs*, **12**, 387 (1966).

Noda, I., Ph.D. Dissertation, Department of Chemical Engineering and Applied Chemistry, Columbia University, New York, NY (1978).

Noda, I. and C. C. Gryte, "Mass transfer in regular array of hollow fibers," *AIChE J.*, **25**(1), 113 (1978).

Noda, I., D. G. Brown-West, and C. C. Gryte, "Effect of flow maldistribution on hollow fiber dialysis—Experimental studies," *J. Memb. Sci.*, **5**, 209 (1979).

Noda, I. and C. C. Gryte, "Composite separation units and their application in dialysis for the isolation of intermediate-sized molecules," *Chem. Eng. Sci.*, **34**, 1545 (1980).

Ohya, H. and S. Sourirajan, "Reverse osmosis seraration of urea in aqueous solutions using porous cellulose acetate membranes," *I and EC Proc. Des. Dev.*, **8**, 131 (1969).

Rony, P. R., "The extent of separation: On the unification of the field of the chemical separations," *Chem. Eng. Prog. Symp. Ser.*, **120**(68), 89 (1972).

Stevenson, J. F., M. von Deak, M. Weinberg, and R. Schutte, "Unsteady state method for measuring the permeability of small tubular membranes," *AIChE J.*, **21**, 1192 (1972).

Viswanadham, R. K. and E. J. Kramer, "Structure of reconstituted collagen hollow fiber membranes," *J. Mater. Sci.*, **10**, 1472 (1972).

Manuscript received June 1, 1978; revision received January 16, and accepted January 20, 1981.

Modeling the Flow of Viscoelastic Fluids Through Porous Media

J. A. DEIBER

and

W. R. SCHOWALTER

Department of Chemical Engineering
Princeton University
Princeton, NJ 08544

A tube with sinusoidal axial variations in diameter has been used as a first step toward modeling the flow channels of a porous medium in such a way that appreciable Lagrangian unsteadiness is present. Experiments with dilute aqueous solutions of a polyacrylamide (Dow Separan AP-30) show that the Lagrangian unsteadiness gives rise to an increase in resistance to flow through the sinusoidal channel relative to that predicted for a purely viscous fluid. The increase in pressure drop can occur as a consequence of fluid elasticity, without any observable secondary flow. At sufficiently high flow rates, secondary flow appears.

SCOPE

In a recent paper (Deiber and Schowalter, 1979) we showed how a technique of geometric iteration could be used to obtain solutions to the Navier-Stokes equation for flow through tubes with sinusoidal axial variations in diameter, where the amplitude of variation is comparable to the average radius. In the present work this technique is extended to flow of viscoelastic fluids. The theoretical results are accompanied by data on pressure drop and streamline profiles for dilute aqueous solutions of polyacrylamide (Dow Separan AP-30).

The research was motivated by a desire to model the flow of viscoelastic liquids through porous materials by means of a geometry sufficiently realistic to include the most important aspects of the flow, but sufficiently simple to be mathematically tractable. We believe that the sinusoidal geometry is an effec-

tive compromise. In particular we wished to determine whether the anomalously large pressure drop observed by several investigators (Marshall and Metzner, 1967; James and McLaren, 1975) was in fact due to the stretching flow imposed by a porous geometry. Our results show that, in contrast to Newtonian fluids, one can indeed obtain a substantial increase in pressure drop without any observable secondary flow in the sinusoidal tube.

CONCLUSIONS AND SIGNIFICANCE

Experiments in a tube with axial sinusoidal variations in diameter have shown that viscoelastic fluids can exhibit substantial increases in pressure drop beyond that expected for comparable viscous fluids. This increase can occur without the inception of secondary flow, which, for the fluids and geometries considered, is a consequence of inertia. The results are important for explanation of the anomalously high pressure drop observed in some cases when viscoelastic fluids flow through porous media. We have shown that in our experiments the increase is caused by Lagrangian unsteadiness due to the axial variations in diameter. Similar unsteadiness, and hence the stretching and compression of fluid filaments, is present during flow through a porous medium.

Computations in which we employed the technique of geometric iteration to solve the nonlinear equations of motion show qualitative agreement with the experimental results.

LAGRANGIAN UNSTEADINESS

Experimental evidence indicates that at sufficient flow rates the energy required to force viscoelastic fluids through packed beds is far greater than one predicts from application of viscometric measurements to a model of the bed as an equivalent bundle of capillary tubes (Marshall and Metzner, 1967; Dauben and Menzie, 1967; James and McLaren, 1975; Laufer et al., 1976; Kemblowski and Dziubiński, 1978; Barboza et al., 1979). The discrepancy is usually ascribed to elastic effects associated with Lagrangian unsteadiness of the flow. We refer, of course, to the unsteady flow experienced by individual fluid elements as they move through interstices between solid particles. However, other sources, such as interactions between the polymer and the solid packing or diffusion due to entropic effects have been cited as factors in at least some of the cases studied (Metzner, 1977).

In the present work our intent was to remove the geometric ambiguities which necessarily attend a porous material, but to retain the feature of Lagrangian unsteadiness. This was done by considering flow through a tube the diameter of which is a sinusoidal function of distance along the tube axis.

Most of the theoretical work on flow of non-Newtonian fluids through periodically constricted conduits applies only to tubes with a diameter variation which is small relative to the average diameter. A typical example is the work of Dodson et al. (1971), who solved for the flow of an Oldroyd fluid through a tube characterized by radius r_0,

$$r_0 = a - \epsilon \cos(2\pi z/\lambda) \tag{1}$$

with $\epsilon << a$.

Experiments with non-Newtonian fluids have been conducted by Porteous (1969) and by Gadala-Maria (1973) for tubes composed of conically shaped diverging and converging sections, and by Franzen (1978) for the geometry used by Payatakes et al. (1973) to simulate a bed of packed spheres.

In this paper we report results for flow of viscoelastic fluids through tubes described by Eq. 1 when the restriction $\epsilon << a$ is not required.

FLOW EQUATIONS AND METHOD OF SOLUTION

It is convenient to rewrite Eq. 1 in the dimensionless form

$$R_0 = 1 - \alpha \cos Z \tag{2}$$

where $R_0 = r_0/a$, $\alpha = \epsilon/a$, and $Z = 2\pi z/\lambda$, λ being the wave length of radius variation. Dimensionless forms of the continuity equation and the equation of motion are, respectively,

$$\frac{1}{R}\frac{\partial}{\partial R}(RV) + \Lambda\frac{\partial W}{\partial Z} = 0 \tag{3}$$

$$W\Lambda\frac{\partial \Omega}{\partial Z} + V\frac{\partial \Omega}{\partial R} - \frac{V}{R}\Omega = \frac{\partial}{\partial R}\left[\frac{1}{R}\frac{\partial}{\partial R}(\tau R)\right] - \Lambda^2\frac{\partial^2 \tau}{\partial Z^2} - \Lambda\frac{\partial}{\partial Z}\left[\frac{N_2}{R} - \frac{\partial N_1}{\partial R}\right] \tag{4}$$

and the dimensionless vorticity is

$$\Omega = \frac{\partial W}{\partial R} - \Lambda\frac{\partial V}{\partial Z} \tag{5}$$

It is assumed throughout that the flow is axisymmetric and that there is no circumferential velocity. Furthermore, the flow is assumed to have the same periodicity as the boundaries. Thus boundary conditions are

$$\begin{aligned} V = W &= 0 && \text{at } R = R_0 \\ V = \partial W/\partial R &= 0 && \text{at } R = 0 \\ V(R, Z) &= V(R, Z + 2\pi) && 0 \le R \le R_0 \\ W(R, Z) &= W(R, Z + 2\pi) && 0 \le R \le R_0 \end{aligned} \tag{6}$$

As a prototype rheological model we have found the contravariant form of the convected Maxwell model to be convenient (Schowalter, 1978). The dimensionless stress components in cylindrical coordinates are

$$\tau + \mathrm{We}\left[W\Lambda\frac{\partial \tau}{\partial Z} + V\frac{\partial \tau}{\partial R} - \tau\left(\frac{\partial V}{\partial R} + \Lambda\frac{\partial W}{\partial Z}\right) - \tau_1\Lambda\frac{\partial V}{\partial Z} - \tau_2\frac{\partial W}{\partial R}\right] = \frac{1}{\mathrm{Re}'}\left[\frac{\partial W}{\partial R} + \Lambda\frac{\partial V}{\partial Z}\right]$$

$$\tau_1 + \mathrm{We}\left[W\Lambda\frac{\partial \tau_1}{\partial Z} + V\frac{\partial \tau_1}{\partial R} - 2\left(\tau\frac{\partial W}{\partial R} + \tau_1\Lambda\frac{\partial W}{\partial Z}\right)\right] = \frac{2\Lambda}{\mathrm{Re}'}\frac{\partial W}{\partial Z} \tag{7}$$

$$\tau_2 + \mathrm{We}\left[W\Lambda\frac{\partial \tau_2}{\partial Z} + V\frac{\partial \tau_2}{\partial R} - 2\left(\tau\Lambda\frac{\partial V}{\partial Z} + \tau_2\frac{\partial V}{\partial R}\right)\right] = \frac{2}{\mathrm{Re}'}\frac{\partial V}{\partial R}$$

$$\tau_3 + \mathrm{We}\left[W\Lambda\frac{\partial \tau_3}{\partial Z} + V\frac{\partial \tau_3}{\partial R} - 2\tau_3\frac{V}{R}\right] = \frac{2}{\mathrm{Re}'}\frac{V}{R}$$

It is convenient to use τ_1, τ_2, and τ_3 to designate dimensionless normal stresses in the axial, radial and circumferential directions, respectively. The Weissenberg number is defined by $\mathrm{We} = \theta Q/a^3$, where θ is the relaxation time in the Maxwell model, and $\mathrm{Re}' = Q/(\nu a)$.

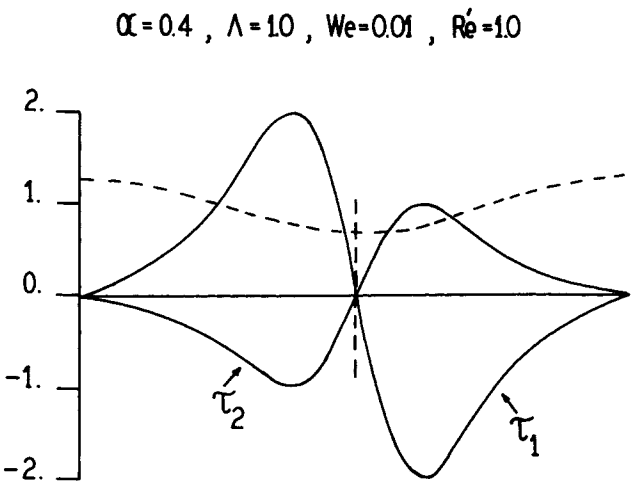

Figure 1. Normal stresses at the tube center for a convected Maxwell model, Eq. 12, with constant θ and μ. Dashed lines indicate the tube wall and location of the minimum tube diameter. Flow is from left to right.

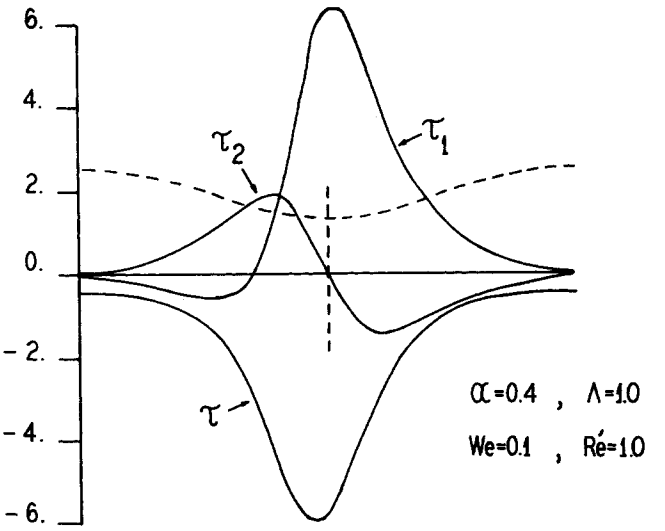

Figure 2. Normal and shear stresses at the tube wall for a convected Maxwell model, Eq. 12, with constant θ and μ. Dashed lines indicate the tube wall and location of the minimum tube diameter. Flow is from left to right.

Following our previous experience with Newtonian fluids (Deiber and Schowalter, 1979), we chose to replace the radial coordinate by a new independent variable

$$\eta = R/R_0(\alpha, Z) \tag{8}$$

and to write the components of velocity in terms of a stream function $\psi(\eta, Z)$, where

$$W = \frac{1}{\eta R_0^2}\frac{\partial \psi}{\partial \eta}$$
$$V = -\frac{\Lambda}{\eta R_0}\left[\frac{\partial \psi}{\partial Z} - \eta(R_0'/R_0)\frac{\partial \psi}{\partial \eta}\right] \tag{9}$$

Resulting equations and boundary conditions are given in the Appendix.

The numerical procedure for solution is similar to that of Deiber and Schowalter (1979) and will not be described in detail. As before, we employed the technique of geometric iteration from a tube with $\Lambda \to 0$ to one with the Λ of interest (see Appendix). The value of $\Delta\Lambda$ was sufficiently large to avoid difficulties from roundoff and truncation errors, but sufficiently small to provide residuals of $0(10^{-3})$ at each iteration for the following periodicity requirements:

$$|\tau^{(n)}(\eta, 0) - \tau^{(n+1)}(\eta, 2\pi)|/\tau^{(n)}(\eta, 0)$$
$$|\psi^{(n)}(\eta, 0) - \psi^{(n+1)}(\eta, 2\pi)|/\psi^{(n)}(\eta, 0) \tag{10}$$
$$|\tau_k^{(n)}(\eta, 0) - \tau_k^{(n+1)}(\eta, 2\pi)|/\tau_k^{(n)}(\eta, 0);\ k = 1, 2, 3$$

The grid was usually constructed with 21 × 41 points for η and Z, respectively. Double precision arithmetic was used on an IBM 360/91. Computation time for results at a specified flow rate was approximately 55 seconds.

With straightforward modifications (Deiber, 1978) the computations were arranged to apply to a model in which the relaxation time and viscosity are dependent on the second invariant of the rate of deformation tensor. We used the White-Metzner (1963) modification of the Maxwell model, for which

$$\theta(\mathrm{II}) = \mu(\mathrm{II})/G \tag{11}$$

is substituted into the contravariant form of convected Maxwell model

$$t^{ij} + \theta(\mathrm{II})\frac{\delta t^{ij}}{\delta t} = 2\mu(\mathrm{II})\dot{e}^{ij} \tag{12}$$

and $\mu(\mathrm{II})$ is given by the power law

$$\mu(\mathrm{II}) = m(\mathrm{II}/2)^{\frac{n-1}{2}} \quad \text{if } \mathrm{II} > \mathrm{II}_0$$
$$\mu(\mathrm{II}) = m(\mathrm{II}_0/2)^{\frac{n-1}{2}} \quad \text{if } \mathrm{II} \le \mathrm{II}_0 \tag{13}$$

The elastic modulus G is taken to be a constant.

COMPUTATIONAL RESULTS

Normal Stresses

Normal stresses show, as one would expect, a cyclic behavior with change in axial position. Representative stress profiles are shown in Figures 1 and 2 for stresses at the tube center and wall, respectively, based upon a convected Maxwell model with constant θ and μ. Qualitatively similar results are obtained when the White-Metzner modification, Eq. 11, is employed.

Some interesting phase relationships occur with changing fluid elasticity. An example is shown in Figure 3. In the figure N^+ and N^- refer to the positive and negative peaks, respectively, of the first normal stress difference N_1 for the convected Maxwell model. ΔN is the phase difference between the axial position where N_1 goes through zero and the position of minimum tube diameter. A positive ΔN indicates that the zero of N_1 is located downstream from the position of minimum diameter.

The experiments described below were not designed to measure normal stress differences, and in any event one would not expect quantitative reproduction of results based on a simple constitutive model. However, it would be reasonable to anticipate qualitatively similar behavior for real fluids.

The possibility of large anisotropy in normal stress components when viscoelastic fluids flow through porous media does not seem to have been noted explicitly before. The result could have a significant effect on the stress in a porous rock formation and, ultimately, on its geometry. Perhaps a highly anisotropic stress could be exploited to achieve an increase in formation porosity, an objective of the so-called "fracture fluids" which are currently used for this purpose.

Shear Stress and Pressure Drop

Cyclic behavior of shear stress under conditions of low elasticity is shown in Figure 2, where We = 0.1. The response changes markedly as the Weissenberg number increases. The stress can be either positive or negative, and maxima and

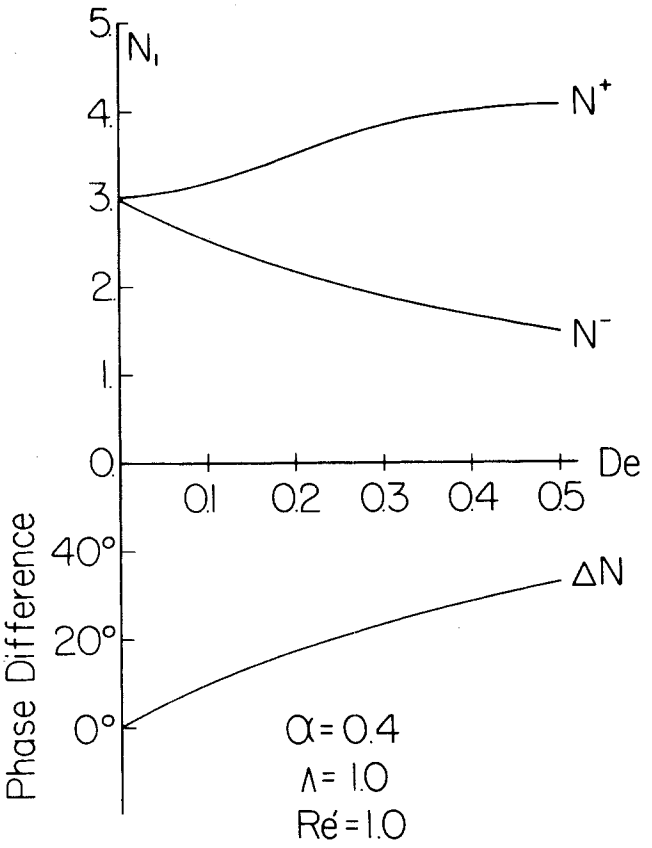

Figure 3. Phase difference and absolute value of positive and negative peaks of first normal stress difference as a function of Deborah number at the tube center for the Maxwell fluid.

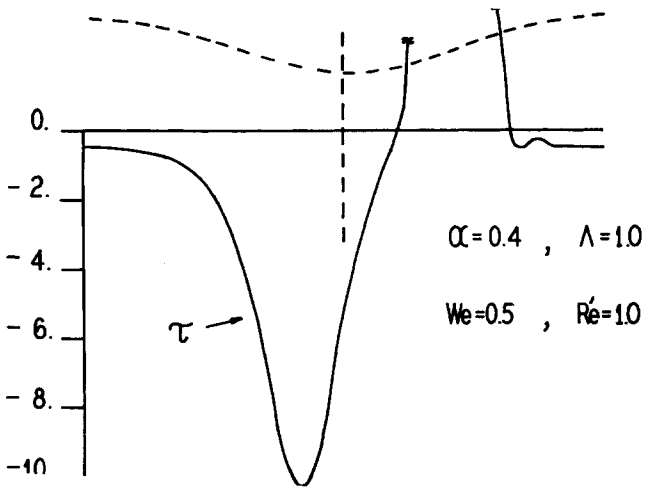

Figure 4. Shear stress profile at the tube wall when solid-like behavior is reached with the Maxwell fluid.

minima in local values of the stress no longer coincide with positions of minimum and maximum diameter. A typical result for a Maxwell fluid is shown in Figure 4 where, for We = 0.5, the maximum value of τ is $0(10^3)$. Because of the wavy profile of the tube, the stress $\tau = t(rz)a^4/(\rho Q^2)$ evaluated at the wall is not, in general, equal to the dimensionless wall stress tangent to the tube surface and in the rz-plane. However, the general features of Figure 4 are also observed if one plots this latter wall stress as a function of axial position. These results are of course a manifestation of the solid-like behavior which is associated with Eq. 12 at sufficiently high Deborah number, defined by De = We Λ. A similar result has already been described for flow through porous media idealized as purely extensional flow in a series of frusta of cones (Marshall and Metzner, 1967). Here again, it is the qualitative resemblance to known behavior that should be emphasized. For example, Laun and Münstedt (1978) have reported results for uniaxial elongational flow of polymer melts showing a substantial increase in elongational viscosity with increasing rate of extension.

We next consider the implications of Figure 4 for pressure drop in porous media. One finds that the dependence of pressure drop on flow rate is nearly independent of elasticity, as measured by De, until, at a critical value of De, the predicted pressure drop rises sharply and the computation is no longer stable. In order to put these results in the context of the usual generalized plots, where pressure drop is expressed as fRe, we have plotted fRe as a function of De in Figure 5 for a fixed value of Re′ = 1, with α as a parameter. As described above, one finds fRe ≅ const. until, at a critical value of De corresponding to the dashed curve in Figure 5, the value of fRe increases rapidly and the computation becomes unstable. One can associate the response to the left of the boundary shown by the dashed curve with fluid-like behavior, transition to a solid-like response occurring at the boundary. An important inference from Figure 5 is the fact that the transition from fluid-like to solid-like behavior is not characterized solely by De, for example by De = 0(1). Even for the simple systems studied, the transition depends strongly on De and the amplitude α. As noted above, the same general results are obtained if one uses the White-Metzner modification of the Maxwell model.

Finally, we note that at sufficiently low Deborah numbers computations indicate inertially induced separation. In these cases separation occurs before the onset of solid-like behavior. An example of the White-Metzner modification of the Maxwell model is shown in Figure 6, which corresponds to the condition for onset of separation.

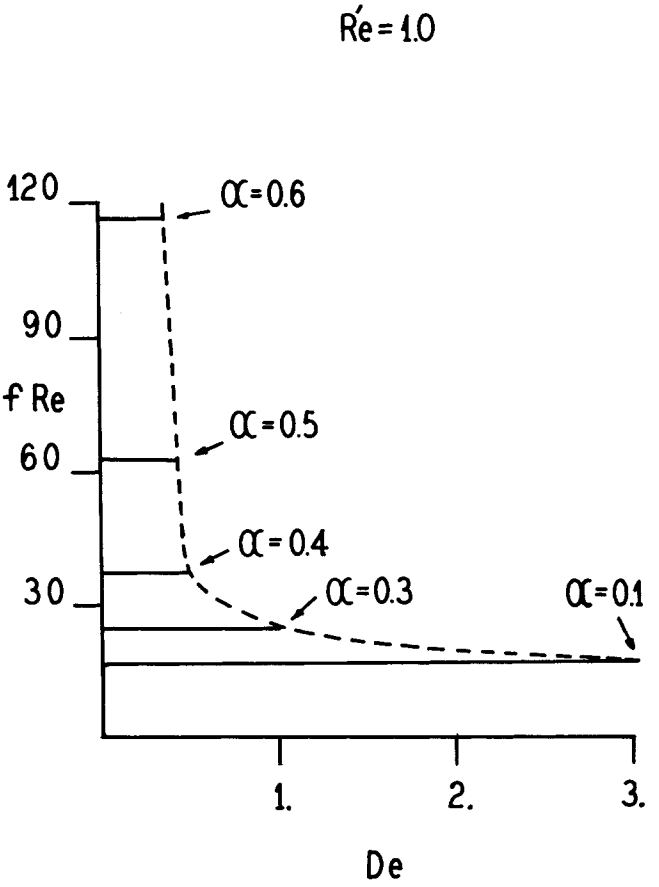

Figure 5. Friction factor-Reynolds number product (fRe) as a function of Deborah number (De = WeΛ) for the Maxwell fluid. Dashed line indicates the onset of solid-like response.

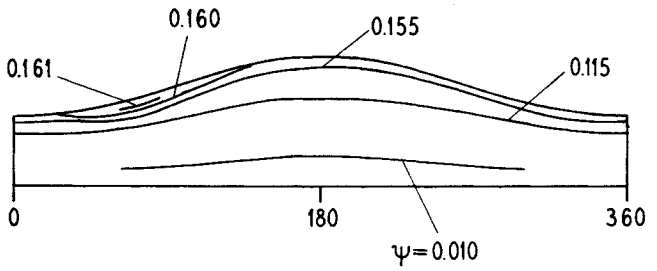

Figure 6. Onset of flow separation as predicted by the White-Metzner modification of the Maxwell model. Parameters are for a 0.1% by weight polyacrylamide solution: $\Lambda = 1.0$, $\alpha = 0.3$, We = 0.346, Re = 39, $n = 0.5$, $m = 0.24$ Pascal s^n.

TABLE 1. DESCRIPTION OF SINUSOIDAL TUBE

a	= 1.0 cm	α	= 0.3
ϵ	= 0.3 cm	L	= 10 λ
λ	= 6.28 cm	L_E	= $L/2$
Λ	= 1.0		

TABLE 2. POWER-LAW PARAMETERS FOR POLYACRYLAMIDE SOLUTIONS (DEIBER, 1978) TEMPERATURE = 19°C

Concentration (Wt. %)	n	m (Pascal s^n)
0.02	0.62	0.04
0.05	0.54	0.10
0.10	0.50	0.24
0.53	0.43	1.5

TABLE 3. COEFFICIENTS FOR EQ. 17

Concentration (Wt. %)	$m'/(2m)$ $(s)^{n'-n}$	$n' - n - 1$	Shear Rate Range s^{-1}
0.05	0.13	−0.40	50-450
0.10	0.20	−0.47	50-270

EXPERIMENTS

The flow system was identical to that used by Deiber and Schowalter (1979). Dimensions of the sinusoidal tube described by Eqs. 1 and 2 are listed in Table 1.

Aqueous test solutions of a partially hydrolyzed polyacrylamide (Dow Separan AP-30) were prepared by standard techniques. Four solutions, prepared by dilution of a 0.53 percent solution, were used in the experiment. Between shear rates Γ of 1 and 10^3 s^{-1} the solutions followed a power-law behavior, which one can write for viscometric flow in cylindrical coordinates as

$$t(rz) = m\Gamma^n \tag{14}$$

with parameters given in Table 2.

An estimate of relaxation time for use with the Maxwell model, Eq. 12, was obtained by setting

$$\theta = \frac{t(zz) - t(rr)}{2\Gamma t(rz)} \tag{15}$$

for a viscometric flow and using the data of Kuo (1973). The first normal stress difference was fit by the power-law expression

$$t(zz) - t(rr) = m'\Gamma^{n'} \tag{16}$$

so that

$$\theta = \frac{m'}{2m}\,\Gamma^{n'-n-1} \tag{17}$$

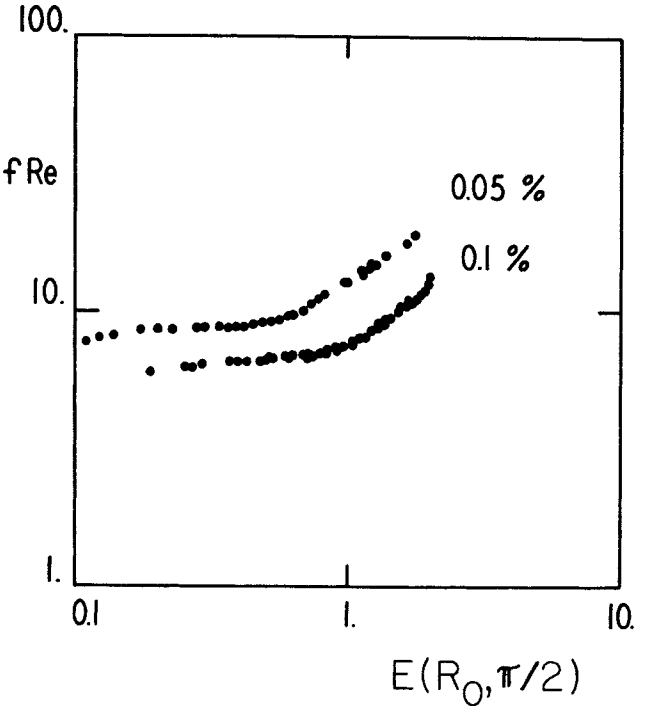

Figure 7. Friction factor-Reynolds number product as a function of the elasticity number. Data (•) were obtained with two polyacrylamide solutions, 0.1 and 0.05% by weight. Geometric parameters are: $\alpha = 0.3$, $\Lambda = 1.0$.

Values of m' and n', and the shear rates over which they are estimated, are presented in Table 3.

One should understand that the empirical fits to data, Eqs. 14 and 17, are not compatible with Eq. 11, in which G was taken as constant. Equation 11, however, was convenient to use for predicting qualitative trends with as few parameters as possible. For simplicity we have characterized the ratio of fluid to process times by an elasticity number

$$E(R, Z) = (\text{II}/2)^{\frac{1}{2}}\theta \tag{18}$$

which is evaluated at the wall and at an axial position $Z = \pi/2$. (Recall from Eq. 2 that $Z = 0$ at the position of minimum radius). The value of $(\text{II}/2)^{1/2}$ is approximated by using the limiting form for $\Lambda \to 0$.

Experimental confirmation of the importance of elasticity is evident from the results shown in Figure 7. For the two concentrations shown, one notes a substantial rise in the product fRe when $E(R_0, \pi/2) = 0(1)$. All of the results shown in Figure 7 are at flow rates below the inception of secondary flow. More conventional plots of the product fRe as a function of Re are presented for the four polyacrylamide solutions in Figures 8-11. The letter "S" denotes the value of Re at which secondary flow was observed with the polystyrene tracer particles (diameter = 500 nm) described in Deiber and Schowalter (1979).

DISCUSSION

As with so many comparisons of theory and experiment with viscoelastic fluids, one is hampered by inability to characterize fluid elasticity with a simple single parameter. (See Astarita, 1979, for a lucid discussion of this problem.) Nevertheless, the convected Maxwell model of Eq. 12 or one of its variations does show the general features which we observed in experiments. The computations displayed in Figure 5 indicate that substantial increases in pressure drop can be caused by elasticity, and that these increases, if they take place at sufficiently low Reynolds number, can occur without any secondary flow. This result is in qualitative agreement with the data shown in Figures 8-10 for flow rates below the onset of secondary flow, indicated by "S" on the figures. The experimentally observed increase in fRe with De is gradual, and quantitative agreement with the computations is lacking. Recall from Figure 5 that computations with the Maxwell model indicate very little change from fRe = constant until the boundary shown by the dashed line in Figure 5 is reached. At that point the product fRe increases by orders

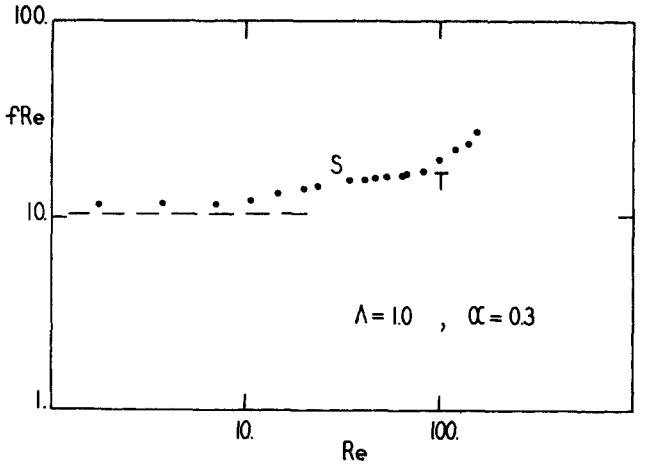

Figure 8. Comparison of theory and experiment for $\alpha = 0.3$, $\Lambda = 1.0$. Data are for a 0.02% by weight polyacrylamide solution. At "T" the flow became turbulent. "S" refers to the point at which a toroidal vortex was visible. Dashed line indicates theoretical prediction for the limit of zero Weissenberg number with the White-Metzner modification of the Maxwell fluid.

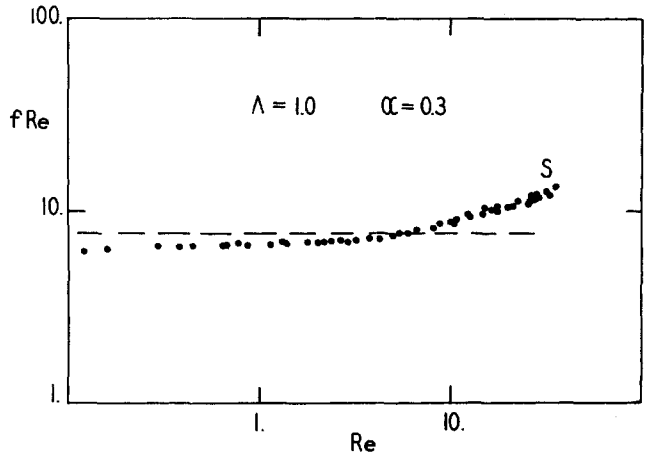

Figure 10. Comparison of theory and experiment for $\alpha = 0.3$, $\Lambda = 1.0$. Data are for a 0.1% by weight polyacrylamide solution.

TABLE 4. FLUIDS AND FLOW REGIMES

Fluid	(Wt. %)	Approximate Reynolds Number at Onset: Elastic Regime	Secondary flow (S)	Turbulence (T)
aqueous polyacrylamide solutions	0.02	7	30	105
	0.05	5	39	—
	0.10	4	38	—
aqueous glycerol solutions	0-90	none	75	580

of magnitude and the computation fails to converge. In Figures 8-11 the dashed line corresponds to the shear thinning viscous limit We $\rightarrow$ 0, i.e., Eqs. 11 and 12 with $G \rightarrow \infty$. Except for the sharp increase to solid-like behavior (Figure 5), the theoretical curves for We > 0 differ very little from those shown unless one reaches a flow rate where inertial effects are also important. One could of course obtain more detailed information by an expansion of the computational program, using a more realistic rheological model and tighter convergence requirements. The cost and effort required were, however, judged excessive for the likely utility of the results.

The results presented here are believed to be the first to show that elastic effects are manifested in an increasing friction factor

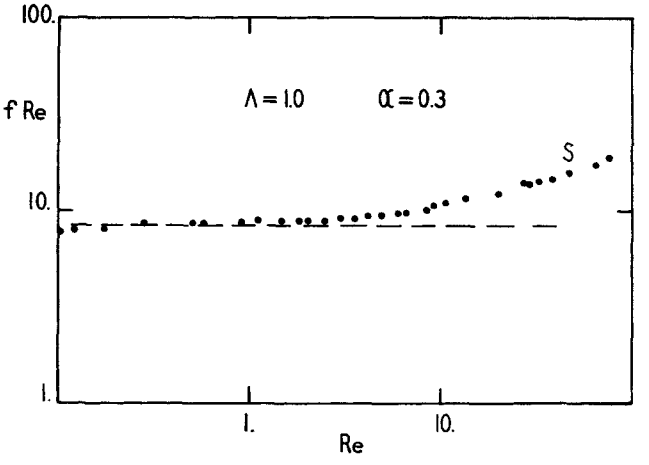

Figure 9. Comparison of theory and experiment for $\alpha = 0.3$, $\Lambda = 1.0$. Data are for a 0.05% by weight polyacrylamide solution.

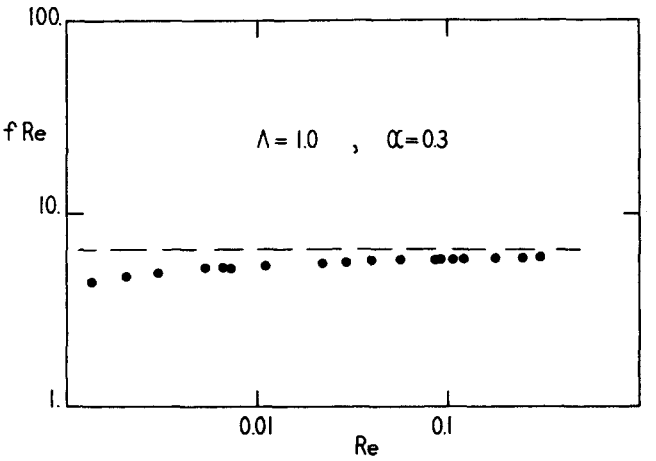

Figure 11. Comparison of theory and experiment for $\alpha = 0.3$, $\Lambda = 1.0$. Data are for a 0.53% by weight polyacrylamide solution.

while the streamlines show no qualitative differences from creeping Newtonian flow. It is recalled that for Newtonian fluids fRe = constant until secondary flow due to inertia is observed (Deiber and Schowalter, 1979). With the polyacrylamides, inertial effects also contribute to separation, but in our experiments separation always occurred at Reynolds numbers larger than those corresponding to the onset of elastic effects. The results, and the contrast with Newtonian behavior, are summarized in Table 4.

One notes from Figures 8-11 that there is a tendency for the measured product fRe to fall below the predicted value for We $\rightarrow$ 0 when Re is sufficiently small. At these low flow rates one reaches the lower limit of applicability of the power-law constants (Table 2) on which the theoretical lines are based. (See also Ashare et al., 1965; and Vaughn and Bergman, 1966.)

It is of some interest to compare computational and experimental results for the onset of secondary flow. The streamlines shown in Figure 6 were computed for the power-law constants m and n which were found experimentally for the 0.1% Separan solution. If one chooses We = 0.346, secondary flow begins at Re = 39, the value which was found experimentally to correspond to the onset of secondary flow. It is possible to estimate a representative experimental Weissenberg number by using Eq. 17 and the maximum wall shear rate at Re = 39. One finds We $\cong$ 1, a value similar in magnitude to that needed in the computations to match the onset Reynolds number. In this particular computation inertial effects are evident at Reynolds numbers below the value at which there is a catastrophic increase in f due to elasticity.

CONCLUSIONS

1. The technique of geometric iteration has been shown to be useful for computing flows through periodically constricted geometries.

2. A tube with sinusoidally varying diameter is a successful model for flow of viscoelastic fluids through porous media in the qualitative sense that one predicts an increase in pressure drop due to fluid elasticity.

3. In contrast to Newtonian fluids, viscoelastic fluids can exhibit substantial departures from the results $f\mathrm{Re}$ = const. as the flow rate is increased, even though no secondary flow is observed.

4. With the viscoelastic fluids and geometries studied, secondary flow is not observed in the experiments until the flow rate exceeds that for which the product $f\mathrm{Re}$ is nearly constant. This behavior is in contrast to Newtonian fluids, for which departure from $f\mathrm{Re}$ = constant is caused by inertia and accompanied by secondary flow.

ACKNOWLEDGMENT

This work was supported by Grant ENG-76-04294 from the National Science Foundation.

NOTATION

a = average radius
De = Deborah number = $\mathrm{We}\Lambda$
$E(R, Z)$ = elasticity number, defined by Eq. 18
$\dot{e}^{ij}$ = rate of deformation tensor
f = friction factor = $\frac{1}{4}\left(\frac{2a}{\lambda}\right)\frac{\Delta P}{\frac{1}{2}\rho\bar{v}^2}$
G = elastic modulus
L = length of test and exit sections
L_E = length of entry section
m = power law coefficient, defined by Eq. 14
m' = power law coefficient, defined by Eq. 16
n = power law index, defined by Eq. 14
n' = power law index, defined by Eq. 16
N_1 = $[t(zz) - t(rr)]a^4/(\rho Q^2)$
N_2 = $[t(rr) - t(\theta\theta)]a^4/(\rho Q^2)$
P = pressure, where ΔP is the pressure loss over one wave length of tubing
Q = volumetric flow rate
R = r/a
r = radial coordinate
Re = Reynolds number = $2^n\pi^{n-2}\mathrm{Re}'$
Re′ = $Q/(\nu a)$ or $\rho Q^{2-n}a^{3n-4}/m$
t^{ij} = stress tensor
$t(zz)$ = axial normal stress
$t(rr)$ = radial normal stress
$t(\theta\theta)$ = angular normal stress
$t(rz)$ = shear stress
$\bar{v}$ = $Q/(\pi a^2)$
v = radial velocity
V = va^2/Q
w = axial velocity
W = wa^2/Q
We = Weissenberg number = $\theta Q/a^3$ or $\theta Q^n/a^{3n}$
z = axial coordinate
Z = $2\pi z/\lambda$

Greek Symbols

α = ϵ/a
Γ = viscometric shear rate
Λ = $2\pi a/\lambda$
ϵ = amplitude of radius variation
η = R/R_0
θ = relaxation time
λ = wave length of radius variation
μ = viscosity
ν = kinematic viscosity = μ/ρ
ρ = density
τ = $t(rz)a^4/(\rho Q^2)$
τ_1 = $t(zz)a^4/(\rho Q^2)$
τ_2 = $t(rr)a^4/(\rho Q^2)$
τ_3 = $t(\theta\theta)a^4/(\rho Q^2)$
ψ = stream function
Ω = vorticity

Subscripts

0 = value at tube wall
i, j = to designate a position in computational grid
k = to designate normal stresses (k = 1, 2, 3)

Superscripts

(n) = value for $\Lambda = n\Delta\Lambda$
= $\frac{d}{dZ}$ unless otherwise designated

Others

II = second invariant of the rate of deformation tensor
II_0 = second invariant of the rate of deformation tensor at which the viscosity becomes constant

$$\frac{\mathfrak{D}t^{ij}}{\mathfrak{D}t} = \frac{\partial t^{ij}}{\partial t} + \sum_k v^k t^{ij}_k - \sum_k v^i_k t^{kj} - \sum_k v^j_k t^{ik}$$

APPENDIX

A coupled set of equations for the stream function and the components of stress is solved simultaneously. From the equation of motion one obtains

$$H_{11}\frac{\partial^2\tau}{\partial\eta^2} + H_{12}\frac{\partial\tau}{\partial\eta} + H_{13}\frac{\partial^2\tau}{\partial Z^2} + H_{14}\frac{\partial^2\tau}{\partial\eta\partial Z} + \tau + H_{15} = 0 \quad \text{(A1)}$$

Components of the stress equations for the Maxwell model are

$$H_{21}\frac{\partial\psi}{\partial\eta} + H_{22}\frac{\partial^2\psi}{\partial\eta^2} + H_{23}\frac{\partial^2\psi}{\partial Z^2} + H_{24}\frac{\partial\psi}{\partial Z} + H_{25}\frac{\partial^2\psi}{\partial\eta\partial Z} + H_{26} = 0 \quad \text{(A2)}$$

$$H_{31}\tau_1 + H_{32}\frac{\partial\tau_1}{\partial Z} + H_{33}\frac{\partial\tau_1}{\partial\eta} + H_{34} = 0 \quad \text{(A3)}$$

$$H_{41}\tau_2 + H_{42}\frac{\partial\tau_2}{\partial Z} + H_{43}\frac{\partial\tau_2}{\partial\eta} + H_{44} = 0 \quad \text{(A4)}$$

$$H_{51}\tau_3 + H_{52}\frac{\partial\tau_3}{\partial Z} + H_{53}\frac{\partial\tau_3}{\partial\eta} + H_{54} = 0 \quad \text{(A5)}$$

Boundary conditions on the stream function are

$$\psi = \partial\psi/\partial\eta = 0 \quad \text{at} \quad \eta = 0 \quad \text{(A6)}$$

$$\psi = 1/(2\pi); \quad \partial\psi/\partial\eta = 0 \quad \text{at} \quad \eta = 1 \quad \text{(A7)}$$

$$\psi(\eta, Z) = \psi(\eta, Z + 2\pi); \quad 0 \le \eta \le 1 \quad \text{(A8)}$$

$$\frac{\partial\psi}{\partial Z}(\eta, Z) = \frac{\partial\psi}{\partial Z}(\eta, Z + 2\pi); \quad 0 \le \eta \le 1 \quad \text{(A9)}$$

Periodicity requirements are also imposed on the stress.

$$\tau(\eta, Z) = \tau(\eta, Z + 2\pi); \quad 0 \le \eta \le 1 \quad \text{(A10)}$$

$$\tau_k(\eta, Z) = \tau_k(\eta, Z + 2\pi); \quad 0 \le \eta \le 1; \quad k = 1, 2, 3 \quad \text{(A11)}$$

For numerical solution of Eqs. A1-A5 the equations were put into finite difference form

$$A_4\tau_{i-1,j} + B_4\tau_{i,j} + C_4\tau_{i+1,j} = D_4 \quad \text{(A12)}$$

$$A_5\psi_{i-1,j} + B_5\psi_{i,j} + C_5\psi_{i+1,j} = D_5 \quad \text{(A13)}$$

$$A_k\tau_{k,i-1,j} + B_k\tau_{k,i,j} + C_k\tau_{k,i+1,j} = D_k;\ \ k = 1, 2, 3 \quad \text{(A14)}$$

Coefficients for Eqs. A1-A14 are listed below.

$$A_1 = -H_{33}/2$$

$$A_2 = -H_{43}/2$$

$$A_3 = -H_{53}/2$$

$$A_4 = H_{11} - H_{12}\Delta\eta/2 - H_{14}\Delta\eta/\Delta Z/2$$

$$A_5 = -H_{21}\Delta\eta/2 + H_{22} - H_{25}\Delta\eta/\Delta Z/2$$

$$B_1 = H_{31}\Delta\eta + H_{32}\Delta\eta/\Delta Z$$

$$B_2 = H_{41}\Delta\eta + H_{42}\Delta\eta/\Delta Z$$

$$B_3 = H_{51}\Delta\eta + H_{52}\Delta\eta/\Delta Z$$

$$B_4 = \Delta\eta^2 - 2H_{11} + H_{13}(\Delta\eta/\Delta Z)^2$$

$$B_5 = -2H_{22} + H_{23}(\Delta\eta/\Delta Z)^2 + H_{24}\Delta\eta^2/\Delta Z$$

$$C_1 = H_{33}/2$$

$$C_2 = H_{43}/2$$

$$C_3 = H_{53}/2$$

$$C_4 = H_{11} + H_{12}\Delta\eta/2 + H_{14}\Delta\eta/\Delta Z/2$$

$$C_5 = H_{21}\Delta\eta/2 + H_{22} + H_{25}\Delta\eta/\Delta Z/2$$

$$D_1 = -H_{34}\Delta\eta + H_{32}\tau_{i,j-1}\Delta\eta/\Delta Z$$

$$D_2 = -H_{44}\Delta\eta + H_{42}\tau_{2,i,j-1}\Delta\eta/\Delta Z$$

$$D_3 = H_{54}\Delta\eta + H_{52}\tau_{3,i,j-1}\Delta\eta/\Delta Z$$

$$D_4 = -H_{15}\Delta\eta^2 + H_{14}(\tau_{i+1,j-1} - \tau_{i-1,j-1})\,(\Delta\eta/\Delta Z)/2 + H_{13}(2\tau_{i,j-1} - \tau_{i,j-2})\,(\Delta\eta/\Delta Z)^2$$

$$D_5 = H_{23}(2\psi_{i,j-1} - \psi_{i,j-2})\,(\Delta\eta/\Delta Z)^2 + H_{25}(\psi_{i+1,j-1} - \psi_{i-1,j-1})\Delta\eta/\Delta Z/2 - H_{26}\Delta\eta^2 + H_{24}\psi_{i,j-1}\Delta\eta^2/\Delta Z$$

$$H_{11} = \eta^2[-1 + (\Lambda\eta R_0')^2]$$

$$H_{12} = -\eta[1 + (\Lambda\eta)^2(R_0''R_0 - 2R_0'^2)]$$

$$H_{13} = (\Lambda R_0\eta)^2$$

$$H_{14} = -2\Lambda^2\eta^3 R_0R_0'$$

$$H_{15} = \eta^2\Lambda\left\{R_0\left[\frac{1}{\eta}\frac{\partial N_2}{\partial Z} - \frac{\partial^2 N_1}{\partial Z\partial\eta}\right] + R_0'\left[\left(\frac{\partial N_1}{\partial\eta} - \frac{\partial N_2}{\partial\eta}\right) + \eta\frac{\partial^2 N_1}{\partial\eta^2}\right]\right\} + \Lambda\eta\left(\frac{\partial\psi}{\partial Z}\frac{\partial\Omega}{\partial\eta} - \frac{\partial\psi}{\partial\eta}\frac{\partial\Omega}{\partial Z}\right) - \Lambda\Omega\left(\frac{\partial\psi}{\partial Z} - \eta\left[\frac{R_0'}{R_0}\right]\frac{\partial\psi}{\partial\eta}\right)$$

$$H_{21} = \Lambda\left\{\eta\left(\frac{\partial\tau}{\partial Z}R_0^2 - \eta R_0'R_0\frac{\partial\tau}{\partial\eta}\right) + R_0R_0'\left(\eta^2\frac{\partial\tau}{\partial\eta} + \tau\eta\right)\right\} + R_0\left(\tau_2 + \frac{1}{\mathrm{WeRe}'}\right) + (\eta\Lambda)^2R_0\left(\tau_1 + \frac{1}{\mathrm{WeRe}'}\right)(2R_0'^2 - R_0''R_0)$$

$$H_{22} = R_0\eta\left\{(\eta R_0'\Lambda)^2\left(\tau_1 + \frac{1}{\mathrm{WeRe}'}\right) - \left(\tau_2 + \frac{1}{\mathrm{WeRe}'}\right)\right\}$$

$$H_{23} = \eta R_0^3\Lambda^2\left(\tau_1 + \frac{1}{\mathrm{WeRe}'}\right)$$

$$H_{24} = -\Lambda R_0^2\left(\eta\frac{\partial\tau}{\partial\eta} + \tau\right)$$

$$H_{25} = -2(\eta R_0\Lambda)^2R_0'\left(\tau_1 + \frac{1}{\mathrm{WeRe}'}\right)$$

$$H_{26} = \eta^2R_0^4\tau/\mathrm{We}$$

$$H_{31} = R_0^3\eta^2/\mathrm{We} - 2\eta\Lambda\left[R_0\frac{\partial^2\psi}{\partial\eta\partial Z} - R_0'\left(\frac{\partial\psi}{\partial\eta} + \eta\frac{\partial^2\psi}{\partial\eta^2}\right)\right]$$

$$H_{32} = R_0\eta\Lambda\frac{\partial\psi}{\partial\eta}$$

$$H_{33} = \Lambda\eta^2\left[-R_0'\frac{\partial\psi}{\partial\eta} - \frac{R_0}{\eta}\frac{\partial\psi}{\partial Z} + R_0'\frac{\partial\psi}{\partial\eta}\right]$$

$$H_{34} = -2\tau\left(\eta\frac{\partial^2\psi}{\partial\eta^2} - \frac{\partial\psi}{\partial\eta}\right) - \frac{2\eta\Lambda}{\mathrm{WeRe}'}\left[R_0\frac{\partial^2\psi}{\partial\eta\partial Z} - R_0'\left(\frac{\partial\psi}{\partial\eta} + \eta\frac{\partial^2\psi}{\partial\eta^2}\right)\right]$$

$$H_{41} = \frac{\eta^2R_0^4}{\mathrm{We}} + 2\Lambda\left[R_0^2\left(\eta\frac{\partial^2\psi}{\partial Z\partial\eta} - \frac{\partial\psi}{\partial Z}\right) - \eta^2R_0R_0'\frac{\partial^2\psi}{\partial\eta^2}\right]$$

$$H_{42} = \eta R_0^2\Lambda\frac{\partial\psi}{\partial\eta}$$

$$H_{43} = -\eta R_0^2\Lambda\frac{\partial\psi}{\partial Z}$$

$$H_{44} = 2(\Lambda\eta)^2R_0\tau\left[\frac{R_0^2}{\eta}\frac{\partial^2\psi}{\partial Z^2} - 2R_0'R_0\frac{\partial^2\psi}{\partial\eta\partial Z} + \eta R_0'^2\frac{\partial^2\psi}{\partial\eta^2} + (2R_0'^2 - R_0''R_0)\frac{\partial\psi}{\partial\eta}\right] - \frac{2\Lambda}{\mathrm{WeRe}'}\left[R_0^2\left(\frac{\partial\psi}{\partial Z} - \eta\frac{\partial^2\psi}{\partial\eta\partial Z}\right) + \eta^2R_0'R_0\frac{\partial^2\psi}{\partial\eta^2}\right]$$

$$H_{51} = \frac{\eta^2R_0^3}{\mathrm{We}} + 2\Lambda\left(R_0\frac{\partial\psi}{\partial Z} - \eta R_0'\frac{\partial\psi}{\partial\eta}\right)$$

$$H_{52} = \Lambda\eta R_0\frac{\partial\psi}{\partial\eta}$$

$$H_{53} = \Lambda\eta R_0\frac{\partial\psi}{\partial Z}$$

$$H_{54} = -\frac{2\Lambda}{\mathrm{WeRe}'}\left(\frac{\partial\psi}{\partial Z}R_0 - \eta R_0'\frac{\partial\psi}{\partial\eta}\right)$$

Derivatives appearing in the above coefficients were evaluated by the Gauss-Seidel iteration technique (Carnahan, Luther and Wilkes, 1969). The algorithm for geometric iteration, where $\Lambda = n\Delta\Lambda$, is

$$\tau_{i,j}^{(n)} = (1/B_4)\,[D_4^{(n)} - C_4\tau_{i+1,j}^{(n-1)} - A_4\tau_{i-1,j}^{(n)}] \quad \text{(A15)}$$

$$\psi_{i,j}^{(n)} = (1/B_5)\,[D_5^{(n)} - C_5\psi_{i+1,j}^{(n-1)} - A_5\psi_{i-1,j}^{(n)}] \quad \text{(A16)}$$

$$\tau_{k,i,j}^{(n)} = (1/B_k)\,[D_k^{(n)} - C_k\tau_{k,i+1,j}^{(n-1)} - A_k\tau_{k,i-1,j}^{(n)}];\ \ k = 1, 2, 3 \quad \text{(A17)}$$

LITERATURE CITED

Astarita, G., "Scale-up Problems Arising with Non-Newtonian Fluids," *J. Non-Newtonian Fluid Mech.*, **4**, 285 (1979).

Ashare, E., R. B. Bird and J. A. Lescarboura, "Falling Cylinder Viscometer for Non-Newtonian Fluids," *AIChE J.*, **11**, 910 (1965).

Barboza, M., C. Rangel and B. Mena, "Viscoelastic Effects in Flow through Porous Media," *J. Rheol.*, **23**, 281 (1979).

Carnahan, B., H. A. Luther and J. O. Wilkes, "Applied Numerical Methods," John Wiley & Sons, Inc., New York (1969).

Dauben, D. L. and D. E. Menzie, "Flow of Polymer Solutions through Porous Media," *Trans. Soc. Petrol. Eng.*, **19**, 1065 (1967).

Deiber, J. A., "Modeling the Flow of Newtonian and Viscoelastic Fluids through Porous Media," Ph.D. Thesis, Princeton University (1978).

Deiber, J. A. and W. R. Schowalter, "Flow Through Tubes with Sinusoidal Axial Variations in Diameter," *AIChE J.*, **25**, 638 (1979).

Dodson, A. G., P. Townsend and K. Walters, "On the Flow of Newtonian and Non-Newtonian Liquids through Corrugated Pipes," *Rheol. Acta.*, **10**, 508 (1971).

Franzen, P., "Strömungskanal mit veränderlichem Kreisquerschnitt als Modell für Zufallsschüttungen gleich großer Kugeln," *Rheol. Acta*, **16**, 548 (1977).
Gadala-Maria, F., "The Study of a Model for the Flow of Viscoelastic Fluids through Porous Media," Department of Chemical Engineering, Princeton University (1973).
James, D. F. and D. R. McLaren, "The Laminar Flow of Dilute Polymer Solutions through Porous Media," *J. Fluid Mech.*, **70**, 733 (1975).
Kamblowski, Z. and M. Dziubiński, "Resistance to Flow of Molten Polymers through Granular Beds," *Rheol. Acta*, **17**, 176 (1978).
Kuo, You-Ti, "The Determination of Second Normal Stress Difference in Viscoelastic Flows," Brown University, Ph.D. Thesis (1973).
Laufer, G., Ch. Gutfinger and N. Abuaf, "Flow of Dilute Polymer Solutions through a Packed Bed," *Ind. Eng. Chem. Fundamentals*, **15**, 77 (1976).
Laun, H. M. and H. Münstedt, "Elongational Behavior of a Low Density Polyethylene Melt," *Rheol. Acta*, **17**, 415 (1978).
Marshall, R. J. and A. B. Metzner, "Flow of Viscoelastic Fluids through Porous Media," *Ind. Eng. Chem. Fundamentals*, **6**, 393 (1967).
Metzner, A. B., "Improved Oil Recovery by Surfactant and Polymer Flooding," D. O Shah and R. S. Schechter, ed., Academic Press, New York, 439-451 (1977).
Payatakes, A. C., Chi Tien and R. M. Turian, "Numerical Solution of Steady State Incompressible Newtonian Flow through Periodically Constricted Tubes," *AIChE J.*, **19**, 67 (1973).
Schowalter, W. R., "Mechanics of Non-Newtonian Fluids," Pergamon Press, London (1978).
Vaughn, R. D. and P. D. Bergman, "Laminar Flow of Non-Newtonian Fluids in Concentric Annuli," *Ind. Eng. Chem. Proc. Des. Devel.*, **5**, 44 (1966).

Manuscript received December 3, 1979; revision received February 5, and accepted February 6, 1981.

Reaction Regimes in Coal Oxidation

A series of seven coals were oxidized in a fixed bed reactor to determine the controlling reaction regimes during mild coal oxidation. The effects of coal porosity and particle size, reactor temperature, and oxygen partial pressure were evaluated. The results show that coal-oxygen reactions are controlled by the rate of internal gaseous diffusion for most coals, and by the rate of chemical reaction for the most porous coal of the set tested. Particle size effects also suggest internal diffusional control. Determinations of cumulative oxygen deposition indicate that surface areas several orders of magnitude greater than the superficial surface can participate in oxidation reactions, putting in doubt the applicability of the model previously derived by Kam et al. (1976a) for external mass transfer control.

G. G. KARSNER
and
D. D. PERLMUTTER
Department of Chemical Engineering
University of Pennsylvania
Philadelphia, PA 19104

SCOPE

The rates at which a variety of coals undergo mild gas phase oxidation were measured in a fixed bed reactor for various reaction temperatures (150 to 300°C), coal particle sizes (−6 + 50 U.S. mesh), and oxygen concentrations (16 to 35 mol percent). Total oxygen consumption, CO_2, CO, and H_2O production, and oxygen deposition rates were determined from gas chromatographic analysis of reactor effluent gases. The experiments identify conditions under which oxidation rate is determined by the rate of gaseous diffusion within the coal particle, or the intrinsic rate of chemical reaction.

CONCLUSIONS AND SIGNIFICANCE

As a result of kinetic studies on seven coals, the oxidation rate was found for most coals to be controlled by internal diffusion, and in the extreme case where rate is independent of particle size, chemically controlled. The earlier model by Kam et al. (1976a) was based on the expectation of very small diffusion rates for gases in coal. As expected for gas-solid reactions, the activation energy for a coal oxidized in a regime of chemical control was found to be almost double the values obtained for coals in the regime of internal diffusional restrictions. At constant reaction conditions, oxidation rate increases linearly with total porosity, but is not proportional to superficial surface area. A significant portion of the internal surfaces of the coals contributes to the overall reaction rate, since cumulative oxygen adsorption during reaction covers an equivalent monolayer surface area orders of magnitude greater than the superficial surface area of the coal. The apparent order of reaction for gaseous oxygen is in the range of 0.70 and does not change significantly with the controlling regime.

Under the mild conditions of oxidation used to reduce a coal's caking propensity, the rate of oxidation depends on the unique combination of chemical composition and physical structure of each individual coal. In the chemically-controlled regime, in the absence of gaseous transport and diffusion limitations, chemical composition and/or the number of reactive sites on the coal surfaces may be expected to greatly influence reactivity; however, because many caking coals are of limited porosity, the physical structure determines the accessibility of these reaction sites to gaseous oxygen. As in any gas-solid reaction, the pore volume distribution of a coal determines the intra-particle diffusional resistance to reactant oxygen and product gases, and therefore the rate of reaction on

Correspondence concerning this paper should be addressed to D. D. Perlmutter.

0001-1541-81-5025-0920-$2.00.